Chemical Engineering Journal 155 (2009) 789–799

Contents lists available at ScienceDirect

Chemical Engineering Journal

journal homepage: www.elsevier.com/locate/cej

Oscillator micromixer

V. Tesař*

Institute of Thermomechanics, Academy of Sciences of the Czech Republic, Dolejskova 5, 182 00 Prague, Czech Republic

ARTICLE INFO

Article history:
Received 20 April 2009
Received in revised form 18 July 2009
Accepted 24 July 2009

Keywords:
Fluidics
Mixer
Micromixer
Oscillator

ABSTRACT

A no-moving-part microfluidic oscillator was developed for mixing two reactants prior to their admission into a microreactor. Instead of the spatial periodicity produced by static mixers, it achieves essentially the same resultant effect by temporal periodicity. In one half of the oscillation period the oscillator directs into its output one reactant, followed by the other reactant during the other half-period. Since the periods are short, the flow in the output channel consists, like in the static mixers, of interleaved layers of the two fluids – here, however, oriented perpendicularly relative to the flow direction. The oscillation depends on dynamic effects so that there is a lower limit of Reynolds numbers at which the device can operate. In experiments this limit was at *Re* ~30, which makes the device well suited for use with present-day microreactors, especially if the mixer is used to supply several reactors in parallel. Data from experiments with two different models agree with very simple kinematic theory for oscillation frequency and for the size of the generated layers in the output.

1. Introduction

Our world is quite likely to be significantly changed, in a number of ways, by the recent advent of microfluidic devices manufactured by methods originally developed for semiconductor electronics [1] – often actually with electronic and fluidic circuitry made together on the same chip. A particularly promising development is that of chemical microreactors [2,3]. A part of the problem of microchemistry is efficient mixing of reactants in the absence of turbulence. Although microdevices with moving components were successfully developed for the purpose, classical mechanical stirring – due to fragility of tiny stirrers and their difficult manufacturing – is not a good idea at the typically sub-millimetre size. Better suited for handling fluids are no-moving-part fluidic devices, based upon clever use of aerodynamic phenomena in fixed-geometry cavities. These "pure fluidic" devices are more robust, reliable, and easier to make. For the mixing, they usually follow the idea of the "static mixers" [4–7] known from the large-scale layouts. Basically, at their output they generate interleaved volumes of the two mixed fluids (or more if the reaction is more complex than binary). The subsequent final elimination of concentration gradients is left to diffusion. Unfortunately, at the low Reynolds numbers typical for microdevices the diffusion is not efficient. The interleaved volumes have therefore to be as thin as possible, with size (thickness) comparable to laminar diffusion length. The "static" micromixers are therefore usually complex spatial structures with small passages through which the fluids are forced to move. In general, such structures are rather delicate and not easy to manufacture.

An interesting alternative, easier and less expensive to make, is to produce the desirable spatial periodicity in a temporal way, by a periodic flow process. The underlying idea is that of no-moving-part fluidic oscillators [1,8,9,21,22]. These exist in two variants. Some, usually configurationally simpler ones (though the theory of their operation is often more complex), are based on hydrodynamic instability. Others use the principle of a fluidic amplifier provided with a feedback loop [1,21]. The instabilities are typically found at Reynolds numbers of the order from $Re \sim 10^1$ to 10^2. The versions with feedback loop operate typically at higher $Re \sim 10^3$ or more, though with some care (usually calling for empirical development to suppressing sensitivity to various side effects, [26]) they may be developed to operate also at lower values $Re \sim 10^1$ or 10^2. At *Re* values below this limit, oscillation may be irregular and even disappear as the available energy is consumed by viscous damping. Though general trend in microfluidics is towards operation at progressively lower *Re* values, contemporary devices are rarely if at all operated below the order $Re \sim 10^2$. This is going to be the standard – at least in pressure-driven microfluidics [1] – also in the foreseeable future. Oscillators operating at these Reynolds number levels are therefore a quite natural choice. Moreover, the mixers considered here, for pre-mixing the reactants before their entering the reactor, are often operated at higher *Re* levels due to their handling larger flow rates because they are often used to supply a group of microreactors operating in parallel. This is typical for the parallel tests performed in combinatorial chemistry [23] and also due to the basic principle of "numbering-up" rather than scaling-up applied to

* Tel.: +420 2 6605 2270.
E-mail address: tesar@it.cas.cz.

1385-8947/$ – see front matter © 2009 Elsevier B.V. All rights reserved.
doi:10.1016/j.cej.2009.07.060

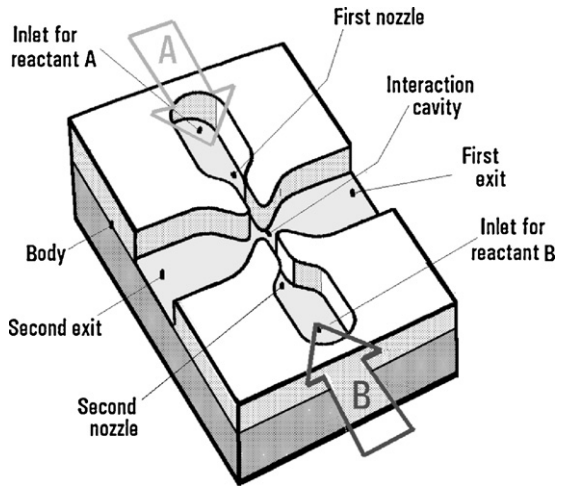

Fig. 1. The discussed microfluidic mixer. Two opposing nozzles, supplied by the two reagents A and B, generate colliding jets which, because of the instability, vibrate transversally. Absence of moving parts and the simple planar geometry, with working cavities of the same depth everywhere, make it suitable for micromanufacturing.

obtain a larger output flow rate of reaction products. The longer distribution channels needed for the transport from the single mixer to many microreactors are actually welcome as they provide the opportunity for the laminar (Fickian) gradient diffusion to perform its job of removal of remaining concentration gradients.

Apart from the mixing, there are other possible useful applications in which two fluids are in mutual contact: an example may be liquid phase extraction with transfer between two immiscible liquids. Other feasibility tests were made, also in an application aimed at putting together small volumes of immiscible liquids, to generate oil droplets in water to make emulsions in food producing applications (salad dressings, ice-creams) [15].

The oscillator device under consideration in the present paper was based on the instability phenomenon found in colliding opposing liquid jets by this author, together with Dr. Tippetts and Dr. Low in 1999 [10] at the University of Sheffield. This was then actually an unwanted regime appearing in a low-Reynolds-number turn-down microvalve [11], which was intended to control steady, non-oscillatory flows. The effect was rather surprising. At first, no feedback mechanism leading to the sustained oscillation was obvious. The effect was believed to be a discovery, deserving an application for a Patent [12] and a communication at a Symposium [13]. Only much later its was learned that the self-oscillation phenomenon in colliding jets was already discussed in literature by Denshchikov et al. [16] in 1983 and mentioned even earlier by Nomoto et al. [17], in 1972. Although remaining relatively unknown, at least in the context of microfluidic mixing, the effect was since then studied by Johnson and Wood [18] and Gregory et al. [19] in 2005.

2. Colliding jets oscillator

2.1. Configuration

The device discussed in the present paper was configured as shown in Fig. 1. It belongs into the category of fluidic oscillators not possessing an apparent, immediately recognisable feedback loop, with the oscillation mechanism based on hydrodynamic instability. The device is extremely simple, containing no-moving-parts. The design is planar, essentially a cavity of constant depth everywhere, closed on top by a flat cover plate – not shown in Fig. 1. The shape, possessing two mutually perpendicular symmetry axes, forms two nozzles opposing one another. The nozzles – each

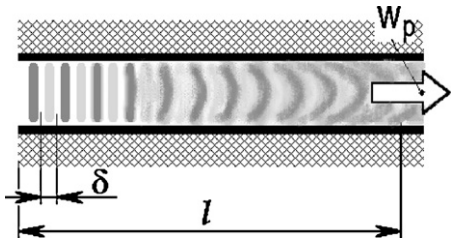

Fig. 2. Schematic representation of the interleaved layers produced by a microfluidic mixer. The illustration attempts to show the blurring and gradual disappearance of the layers due to diffusion.

connected to the supply of one of the two reactants – generate colliding fluid jets. In a certain *Re* range the jets enter a self-excited transversal periodic oscillation regime. The symmetric shape with two output channels means a single mixer supplies two microreactors.

The mixer generates in the exit channels essentially the same result as produced by the "passive static mixers" – the devices tracing their origin to an invention patented in 1965 [24] and applied at the microscale as described e.g. in Ref. [4] or [7], or produced by other, less known types such as, e.g. the vortex mixer [12]. In these devices the output flow in the exit channel(s) consists of interleaved layers or lamellae of the two fluids. Contrary to most static mixer principles, where the generated neighbouring small volumes are elongated in the direction of the flow, in the present case the layers are oriented perpendicularly, Fig. 2, to the channel axis.

Existing literature mentions large-scale colliding jets used in mixing application [20], but in that case, due to the stochastic character of turbulence, the jets did not exhibit the coherent oscillation which is used in the present case.

The mechanism of lamellae formation in the oscillator from Fig. 1, with the transversal oscillation of the two jets, is shown schematically in Fig. 3. While one of the jets, in Fig. 1 the one from the supply terminal A, is deflected to the left-hand side, the other jet, supplied from B, is directed to the right-hand side. The oscillation half-period lasts long enough for both length segments of the two jets reaching up to the opposite side of the interaction cavity. During the subsequent half-period the jets are switched and deflected to the opposite sides. Their segments formed in the previous half-period are shifted away, into the exit channels, where they formed the newly formed lamellae. Of course, the actual motions are not such simple sideways shifts. Due to the jet flow motions

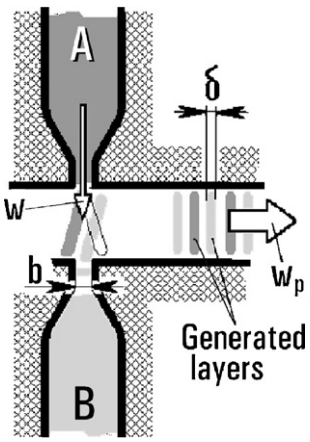

Fig. 3. Drastically simplified schematic representation of the formation, by alternating sideways deflection of the jet segments leaving the nozzles, of the interleaved layers – or lamellae – of the two reagents A and B.

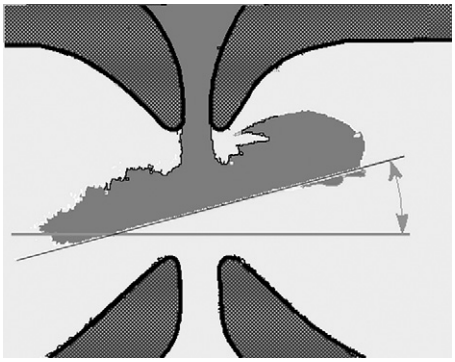

Fig. 4. Photograph of steady asymmetric non-oscillating flow at very low $Re = 18$ in the bistable asymmetric bifurcation regime in the colliding-jets valve [11]. Original colour picture was processed by posterization – drastic reduction of the colour palette to mere two hues – which was rather easy in the regime with very slow laminar diffusion of the dyed fluid.

the lamellae are deformed. Even more pronounced deformations are due to the inevitable vortical character of the motions. Nevertheless, the idealised picture shown in Fig. 3 is a useful starting point for further considerations – in particular, the widths δ of the lamellae in parallel-walls channel are seen in Fig. 3 to be essentially comparable to the jet widths. In the investigated design, as shown in Fig. 1 however, the exit channel walls are divergent so that the channel width – and, consequently, length of the lamellae – increases in the flow direction. The elongation makes the lamellae thinner.

In some microfluidic static mixers, the lamellae in the output flow are lead for repeated processing into another mixer stage – usually applying of the same layer-generating principle at a smaller scale. This leads to fragmentation of the lamellae into smaller yet volumes. This may be done also here (as specifically mentioned in the original Patent Application [12]) but generally is not found necessary in the present case: the generated layers oriented perpendicularly to the flow direction are elongated (and thus become thinner) due to their deformation into the "half-moon" shapes, gradually growing in their lengths, due to the typical velocity profile shapes of the laminar flow. This is accentuated by the typical length of the channel leading from the micromixer to the microreactor - the length that has to be of considerable anyway to provide the opportunity for the rather slow Fickian mixing.

2.2. Laboratory models

The oscillatory unsteadiness of colliding flows was encountered in flow visualisation studies of scaled-up models of microfluidic turn-down valves, developed for control of flow rate of reaction products from a chemical microreactor. At the very low Reynolds numbers, at which this valve was to operate, fluidic vortex-type valves otherwise used for no-moving-part flow turning-down [1] cease to be useful. The developed valves therefore tested another principle – "plugging" the exit [25] by an opposing jet of control fluid, Fig. 4. The geometry of this valve was the starting point in the design of the oscillator mixer, which differs mainly in the symmetry (in the valve the width of the control nozzle, at the top in Fig. 4, was asymmetrically smaller).

Developing the oscillator was guided by the opportunity to apply it for mixing hydrogen and carbon monoxide in a microfluidic sampling unit for testing catalysts for Fischer-Tropsch synthesis [14]. The development – like in the microvalve case – was guided by data and experience gained in visualisations of water flow in scaled up laboratory models. Data acquisition was mainly by video recording the flowfield, made observable by addition of dye to the water supplied to one inlet while the water in the opposite inlet was clear. Velocities were measured by tracing, in the video frames, progression of a particle carried with the fluid. There are several good reasons for development work at the enlarged scale and one – in spite of the intended application to mix the two gases - working with water. Besides the scaling-up making the model easier to make by standard manufacturing methods (avoiding the complications associated with the microscale) and the accessibility for changing the geometry if required, this approach brings the advantage of significantly slower modelled time.

While the condition for similarity of steady flows is generally known to be the equality of Reynolds number Re

$$Re = \frac{bw}{\nu} \tag{1}$$

where b (m), Fig. 5, is the width of the nozzles, w [m/s] is the mean velocity in the nozzle exit, and ν (m^2/s) is kinematic viscosity of the fluid – similarity of periodic processes (not influenced by moving mechanical components) requires identical value of Stokes number

$$Sk = Re\,Sh = \frac{f\,b^2}{\nu} \tag{2}$$

a product of Re and Strouhal number

$$Sh = \frac{f\,b}{w} \tag{3}$$

where f (Hz) is the frequency of oscillation.

If the length scaling factor is Λ

$$\Lambda = \frac{b}{b_\mathrm{m}} \tag{4}$$

where b_m is the model nozzle width, then the time scaling factor, due to Eq. (2), is

$$\tau = \frac{f}{f_\mathrm{m}} = \Lambda^2 \frac{\nu}{\nu_\mathrm{m}} \tag{5}$$

where f_m is the frequency in the model experiment. Obviously, the Stokes number scaling leads to operating the water model at a frequency much lower and therefore easier to record. At the typical water temperatures during the model visualisation experiments, the water viscosity was in the vicinity of

$$\nu_m = 1.25 \times 10^{-6}\,\mathrm{m^2/s} \tag{6}$$

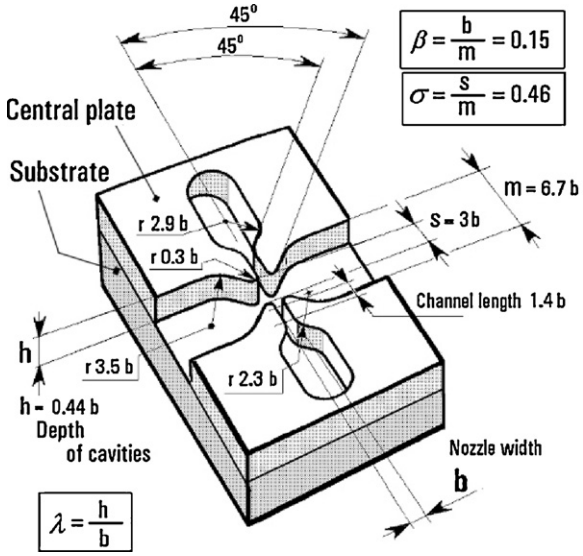

Fig. 5. Geometry of the first laboratory model M1 – scaled up to nozzle widths $b = 3.4$ mm – as used in the initial experiments. The cavities were made by laser cutting in 1.5 mm thick perspex (PMMA) plate.

while the typical value of viscosity of the synthetic gas mixture is 40 times larger

$$\nu = 50 \times 10^{-6}\,\mathrm{m}^2/\mathrm{s} \quad (7)$$

Conditions in the mixer, with the two different fluids, is complicated; nevertheless it is indicative of the model test conditions that in the model scaled up $\Lambda = 10$ times the processes, according to Eq. (5), would be as much as $\tau = 4000$ times slower.

In a binary mixer in general, supplied by two different fluids having different viscosities, two different Reynolds numbers should be in principle stated. This was not a problem here, where only single *Re* value Eq. (1) sufficed for characterisation. The ratio of the two flow rates was invariant, fixed by the stoichiometric requirements of the chemical reaction in the connected microreactor. Moreover in the discussed flow visualisation investigations, the same fluid – water – was supplied into both nozzles. The change in properties (density, viscosity) due to addition of the very small amount of the very powerful Victoria blue dye was checked and found negligible.

Several laboratory models were used. The two most important ones are described here as M1 and M2. All were made by removal of material in a relatively thin plate, which was covered from top by flat cover plate and on the bottom side by flat surface of a substrate. To make possible the flow visualisation, both cover plate and the substrate were made of transparent material – polymethylmetacrylate PMMA. The shape of the removed part of the central plate between them, was in all models mutually geometrically similar – as defined by the relative dimensions in Fig. 5. With the oscillatory mechanism not well understood and the time available for the mixer development limited, there was no opportunity for testing any departures from the shape that was found able to produce the oscillation.

The first model M1, arranged as shown in Fig. 5, was investigated using the test rig originally made for experiments with the turn-down microvalve and shared with it also the manufacturing method of the cavities made by laser cutting in a $h = 1.5$ mm thin PMMA plate. Also the nozzle width $b = 3.4$ mm was the same. It operated successfully, though not at very low *Re* values. The oscillation ceased to be regular as Reynolds number was decreased towards $Re = 100$. At and below this value the oscillation ceased completely. Nevertheless, this was acceptable using the same geometry scaled down to the for the Fischer-Tropsch synthesis tests mixer [14] as shown in Fig. 6.

The small nozzle exit aspect ratio $\lambda = h/b = 0.44$ did not earlier cause troubles in the turn-down microvalve. In the oscillator, however, it became soon obvious that the small value leads to strong damping of the oscillatory motions by the inevitably large friction on both the top cover plate and the substrate plate. In fact, this suppression of the tendency to oscillation was a welcome stabilising effect on the operation of the colliding-jets valve in which flow pulsation was undesirable. Now, however, the inability to oscillate at small Reynolds numbers was an obstacle in the way towards generating very small mixed fluids lamellae in the exit. This was, fortunately, not a serious problem in producing the syngas, because thanks to the extreme molecular diffusivity of hydrogen the very thin lamellae were not necessary.

To investigate the possibilities of mixing other, less diffusive fluids, a new family of models was later developed. Of them, particular mentioning deserves the second model M2, as shown in Fig. 7, with its absolute dimensions presented in Fig. 8. Essentially, these later models were smaller than M1. With newly acquired camcorder lens it became possible to video record processes of physically smaller size. In the model M2 the nozzle width was $b = 1.0$ mm. The shape of the cavities, as presented in Fig. 8, agrees in the critical central part with the geometry as presented in Fig. 5, but the shapes of outer parts now corresponded to the oscillator from Fig. 6. Like those, the cavities were made (by Microponents Ltd., Birmingham) by etching

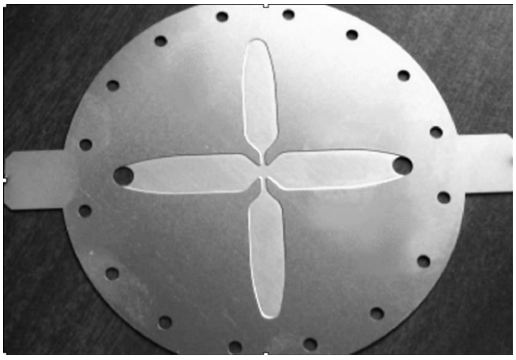

Fig. 6. The mixer with geometry corresponding to the first model M1 as used in the catalyst combinatorial testing facility built for IAC – Institute of Applied Catalysis, London. It supplied 16 reactors performing simultaneous Fischer-Tropsch processes [14]. To withstand the high temperature and pressure levels, the cavity was made by etching in stainless steel foil. No flow visualisations were planned so that there was no need for a transparent substrate.

in stainless steel foils. They were, however, now etched through. Not only this made again possible the visualisation of the flow in transmitted light. They could be used in a stack consisting of several foils on top of one another. This new feature stemmed from the recognition of the strong influence of the nozzle aspect ratio $\lambda = h/b$ on the minimum *Re* value at which the self-excited oscillation remain reliable. The total height h (and hence the aspect ratio λ) of the cavities could be now varied by changing the number of

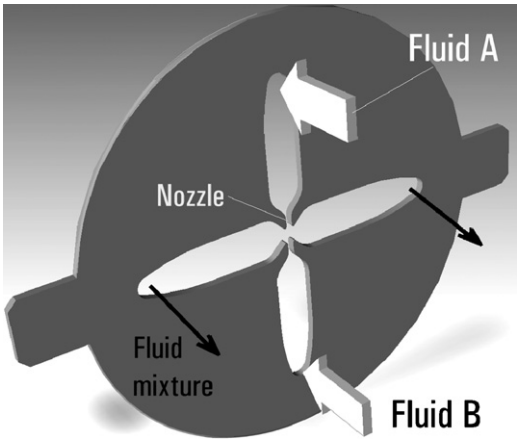

Fig. 7. The stack of the stainless steel foils in which were made – by through etching – the cavities of the second laboratory model M2. The foils were of circular shape, with extensions for mutual foil positioning on both sides. Again, the cavities were closed by flat perspex (PMMA) plates so as to make observable the motions in the cavities, visualised by addition of dye to fluid B while the other fluid A remained clear.

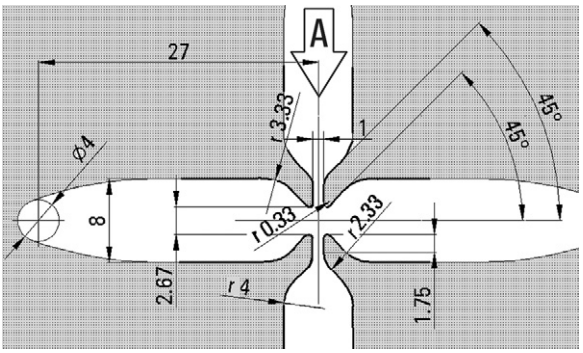

Fig. 8. Geometry of the cavities in the test model M2, made by etching.

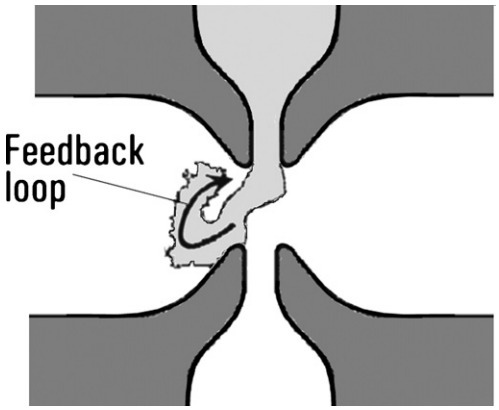

Fig. 9. Posterisation (reduction of the number of colours) helped to identify the feedback loop, necessary for maintaining the self-excited oscillation.

the foils in the stack. Most tests were made with stacks containing either 5 or 10 foils, so that the aspect ratio was either $\lambda = 1.25$ or $\lambda = 2.5$, respectively – the values evidently much larger than in the model M1. As could be expected with the higher aspect ratio, the oscillation persisted when the flow rate was decreased, to significantly lower Reynolds numbers. There were oscillation at *Re* as low as *Re* = 30 observed with $\lambda = 2.5$, though below about *Re* = 50 the oscillation ceased to be regular and reliable and most experiments were performed at slightly higher flow rates.

3. Experiments: flow visualisation

3.1. Identification of the feedback mechanism

Available experimental equipment made possible two forms of investigations: observations of the flowfield, visualised by dyeing one of the mixed fluids, and measurements of the oscillation frequency as a function of the supplied water flow rate. Unfortunately, the available time for performing the experiments did not admit a completely systematic investigation. It was necessary to concentrate just on the conditions of immediate interest for the particular applications.

A useful method of processing the flow visualisation video images prior to analysing them was "posterising", drastic reduction of the original continuous colour palette [27,29]. This procedure consisted first of identifying isophote contours in the image and then filling a constant colour (or shade of grey) between two neighbouring isophotes. The original continuous distribution of colours (or shades) was thus replaced by a limited number of equal-colour regions. The shapes of these regions provide an interesting information about the character of the flowfield – perhaps somewhat surprisingly, considering the fact that this procedure actually decreases the amount of information contained in the image. In this particular case of the problem of mixing two fluids, very useful information about the motion of the two mixed components was gained by limiting the number of colours to mere two (Figs. 4, 9 and 10). The resultant two areas with different colours were and their delimiting boundary roughly thus provide a cue about what volumes are occupied, at a particular instant of time, by the two fluids. The example of the posterised image in Fig. 9, was used for identification of the feedback loop action – which, is generally a necessity for presence of self-excited oscillation – but is rather elusive in the discussed oscillator, where the character of the feedback action was not obvious.

The rather surprising aspect of the oscillation mechanism is the nature of the force that causes the jets to change their flow direction and deflect. Because of the symmetry of the solid boundaries, there is no obvious reason for an asymmetric, sideways motion of the jets. Indeed, at very low Reynolds numbers, *Re* < 10, the flowfield is always perfectly symmetric – and there is no oscillation. The necessary condition the unsteadiness is symmetry breaking. This, in its earliest stage, leads first to steady asymmetry, as demonstrated for *Re* = 18 in Fig. 4. Observation of the flowfield shows, that roughly above this value, if the Reynolds number is increased further, the flowfield becomes complicated by emergence and presence of vortical motion. A certain role in the subsequent development of the flowfield may also play the fluidic resistances of the exit channels. If the deflected inclined jet cannot freely move away through the exit, it is turned back and is forced to form a loop, as shown in the posterised video frame in Fig. 9. Loop formation is very probably associated with the tendency of shear flows rolling up through the Kelvin-Helmholtz instability [28].

An important effect then taking place is the returning direction of the moving tip of the jet. As the jet is turned back, it is seen in Fig. 9 to act on itself in its most sensitive location – in the region where the jet leaves the nozzle. That an action in this location suffices to deflect the jet is a well-known fact, employed in the vast category of fluidic jet-deflection amplifiers (cf., e.g., their description in Ref. [1]). Here the deflecting action at the nozzle exit is applied to the jet itself. It is forced back to return into its original flow direction but overswings – because of fluid inertia – and becomes deflected to the opposite side. It seems quite probable that this is the reason why the colliding jets oscillate.

3.2. Frequency for unequal momentum rates

In the first flow visualisation experiments, with the model M1, two oscillatory regimes were video recorded, with the images then analysed one by one. These experiments were marked G and H. The conditions in both experiments were quite similar, Reynolds numbers for the flows of fluid B were *Re* = 410 in the G case and *Re* = 415 in the H case. The difference between them was asymmetry of the flow were significant asymmetry of the flows in the latter case: while in the case G the ratio of nozzle exit velocities *w*A/*w*B was 1.1, in the case H it was 1.81. In the mixer applications where flow rates of the pre-mixed reactant are determined by the requirements of stoichiometry and reactants have different physical properties, the momentum fluxes in the two nozzles cannot be expected to be equal. The symmetric situation of the equal jet momentum flow rates in most subsequent experiments, as a result, are an exception

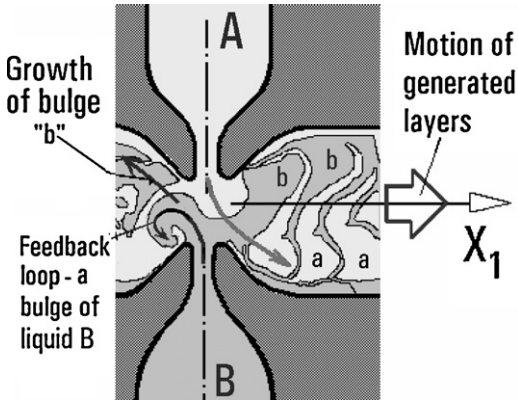

Fig. 10. A posterised picture from the video record frame of oscillation in the regime G in the model M1. The darker arrow at left was drawn to indicate the progressively increasing the darker region filled by the fluid B. Visible asymmetry of the left and right side of the generated shapes is due to unequal hydraulic resistances of the different tubings connected to the exits.

rather than the normal state. The asymmetry influences the oscillation mechanism and the two experiments, G and H were made to investigate this effect. Of course, in the geometrically symmetric model operated with water in both nozzles, the only possibility how to vary the momentum flux ratio was changing the ratio of the two jet exit velocities, wA/wB.

It was found that the resultant highly eccentric position of the mean stagnation point in the case H leads to less regular oscillation. In the extreme cases of $|wA/wB| > 2$ the oscillation may be halted altogether. This not happen in the experiment H. What was found was a significant decrease of the oscillation frequency, which resulted in Strouhal number – Eq. (3) – equal to $Sh = 0.022$ – nearly mere one half of $Sh = 0.041$ found in the experiment G with nearly momentum flow rates.

3.3. Bulging and deformation of the feedback loop

Another information gained from detailed observations of the visualised oscillation is the character of the jet flows, which in its details differs from the simplistic introductory idea presented in Fig. 3. The trend towards vortical motions [29] is reflected in the video clip images in formation and growth of bulges, which may be explained with help of Fig. 10. This illustration presents the central part of a video frame, showing flowfield inside the model M1 during the experimental run G. The image was processed by the posterisation. In the situation shown there, the flow of the fluid B, made visible by dye addition and shown here in a darker shade of the grey colour, is seen to be bifurcated into the left-hand branch and right-hand branch. The branch on the left is more intensive and is deflected less. Its smaller deflection angle relative to the original direction of the outflow from its nozzle contrasts with the practically perpendicular flow direction on the right. The necessity to move at a larger turning angle makes the right-hand branch weaker. At left, the growing darker jet of fluid B visibly cannot continue unobstructed into the left-hand exit channel. It encounters there the previously produced interleaved layers and this forces this branch to turn back. It is this branch that obviously forms the feedback loop, as already discussed in association with Fig. 9. The tip of the darker left-hand jet branch loop is in Fig. 10 just about going to act back on the upwards-directed jet near its nozzle exit. This loop region is seen in the posterised image as the bulge "b". Before the jet turned back manages to change the direction of the exit flow, it forms a bigger bulge "b", which gradually grows, because it is supplied by additional fluid B leaving the bottom nozzle. At the same time a similar gradually bulging loop of the lighter-shade fluid A is formed at right, downstream from the exit from the upper nozzle. When the feedback loop action becomes significant, it constricts the bottom part of the bulge while its bent part near the jet tip remains wide.

A consequence of this process is seen at the right-hand part of the illustration, where similar bulge formations and their later constrictions took place in previous oscillation periods. As a result of these previous cycles, it is possible to recognise at the right-hand side the residua of the wide parts of the bulges "b". They are mutually separated by the interleaving thin regions of the light-grey fluid A which has left the top nozzle and later became constricted.

This mechanism of bulge formation and growth is the dependent on the hydraulic resistance which the deflected jet meets in the exit channel. This fact was recognised later and in most of these experiments the resistances were not adjusted and were not the same in the two exits. As a result the formation of the layers was different at the two sides. Structures formed in the exit channel on the left-hand side were far from a perfect mirror image of what is seen at right – this is remarkable, e.g., in Fig. 11.

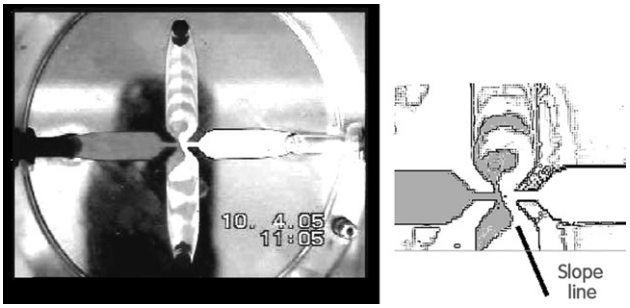

Fig. 11. Left: frame from video clip showing the oscillation in model M2. Right: enlarged and posterised central part of the picture with the thick line indicating the positive slope of the demarcation line on the nozzle axis.

3.4. Motions of the demarcation line

The mechanism of the oscillation of the colliding jets is quite complex. Both jets bifurcate into two branches, directed into opposite directions, and the directions of their motion vary substantially during the oscillation cycle. What was clearly seen and relatively easy to follow in the sequence of Images – especially when posterised to only two colours (or shades of grey in the pictures shown here), was the demarcation line between the two fluid regions near the location of the jets' mutual impingement. The branches of the bifurcated jets in this location followed and were nearly parallel there to the demarcation line. While in the steady flows at extremely low Reynolds numbers the bifurcation is balanced, with equal intensity of the two branch flows, in the oscillatory regime the division is unequal and varies in the course of each oscillation cycle. The consequence are the varying feedback-loop bulges seen in the visualisation pictures, growing alternatively on the opposite sides of the axis of symmetry of the nozzles and then becoming detached and flattened. In this process of bulges growth and deformation, the demarcating line between the two fluids A and B undergoes visible changes. Most apparent are the changes of its slope.

Of course, static pictures cannot convey the impressions obtained by observations in the video clips of the bifurcation, formation of the bulges, their elongation, deformation, and final change into the lamellae. Some idea may be nevertheless gained from the following three frames, presented in Figs. 11–13, taken from one of the video clips. They show the flowfield inside the oscillator mixer at three different instants of time in the same oscillation process. The experiment was made with the model M2 at velocity ratio very near to $wA/wB = 1$. Each of the frames is here accompanied, at the right-hand side, by an enlarged posterised picture of the

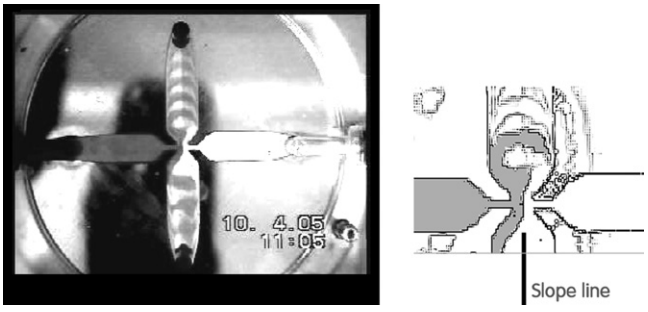

Fig. 12. Left: frame from video clip showing the oscillation in model M2. The same experiment, picture taken at a different time than the one in Fig. 12. The dark area at the bottom and centre of the image is the reflection of the camcorder from the glossy top surface of the model. Right: enlarged and posterised central part of the picture with the thick line indicating the zero slope of the demarcation line on the nozzle axis. The dark coloured jet at this phase bifurcates.

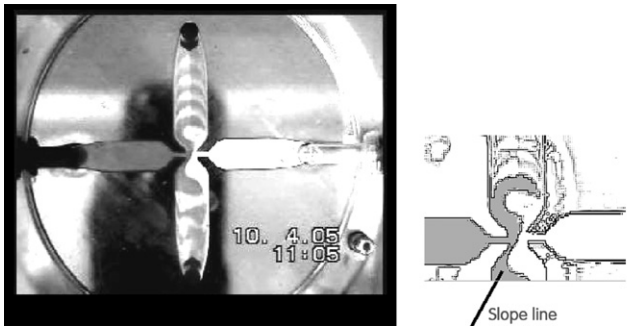

Fig. 13. Left: frame from video clip showing another phase of the oscillation in model M2, again during the same experiment as in Fig. 11. Right: enlarged and posterised central part of the picture with the thick line indicating the negative slope of the demarcation line on the nozzle axis. The downwards directed branch of the bifurcated dark-colour jet is constricted and loses its importance.

central interaction region. Drawn in these accompanying illustrations is a thick black line, indicative of the demarcation line slope. The examples presented in Figs. 11 and 13 were selected so as to show approximately the states with the extreme positive and negative inclinations. In Fig. 12 is shown the transition between the two extremes – the intermediate state with zero inclination of the demarcation line. Only in this state there is a temporarily balanced bifurcation into jet branches of nearly the same intensity. Here, however, it is not a steady balanced state – it is an instant in dynamic unsteady regime with the jet actually overswinging from one side to the opposite one – a process based on fluid inertia.

As already mentioned, only later was recognised the fact that for symmetry of the mixing process it is important to pay attention to the hydraulic conditions in the exit tubing leading the mixture from the exit channels of the model. In the experiments Figs. 11–13 are seen the consequences of the unbalanced exits (the flow in the exit directed down in the picture is visibly faster than the one leading up from the interaction region). What was worse, subsequent analysis indicated that the tubing formed a U-tube with its own resonance that, in some regimes, could interfere with the investigated process. Another interesting aspect were the discernible changes of the stagnation point position – varying distance x in Fig. 14. These motions are indicative of the periodic variations of the relative intensities of the two branches of the bifurcating jets and this made them an interesting object of a detailed study. The study was made using the video clip of the experimental run G with the larger model M1. Both parameters defined in Fig. 14 were found to vary in a practically harmonic manner – although there are some demonstrably systematic deviations, the most obvious that of the point "e" Fig. 16, which may suggest a more complex spectrum.

It was actually in the diagrams like Figs. 15 and 16 that the oscillation frequency $f = 1.46$ Hz (and the parameters computed from it, like $Sh = 0.041$, mentioned above) were determined. Interestingly, this frequency is very low compared with the characteristic frequency $w/b = 35.3$ Hz. Indeed, the surprisingly low Strouhal number $Sh = 0.041$ should be noted as a value a decimal order of magnitude smaller than what would correspond to the basic varicose ("columnar") instability of a fluid jet. This indicates the feedback mechanism is here different – a suggestion also supported by the fact of substantially decreased Sh due to momentum fluxes unbalance in the experiment H.

4. Analysis

4.1. Simple kinematic theory for frequency

Validity of the hypothesis about the feedback mechanism, based on the idea of the jet forming a loop derived from inspection of

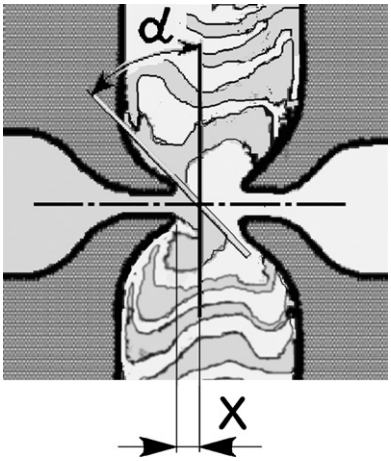

Fig. 14. The two measured geometric parameters evaluated in the demarcation point on the common axis of the two nozzles in the individual frames of the video clip record of the experiment G with model M1. The parameters are the inclination angle α and the distance x form the left-hand nozzle.

images like Fig. 9, was tested by evaluating the oscillation frequency that would follow from this hypothesis.

With the knowledge of the velocity of the jet, the oscillation period may be evaluated from the time the jet requires to traverse the loop path. Of course, an exact evaluation of the path length and velocity (varying in time) would be extremely complicated. An approximate theory was therefore set up arriving at acceptable order-of-magnitude results under the drastically simplifying assumption of a constant jet velocity w (evaluated from the supplied flow rate and nozzle exit cross section) and the approximated simple expression for the jet path shown in Fig. 17.

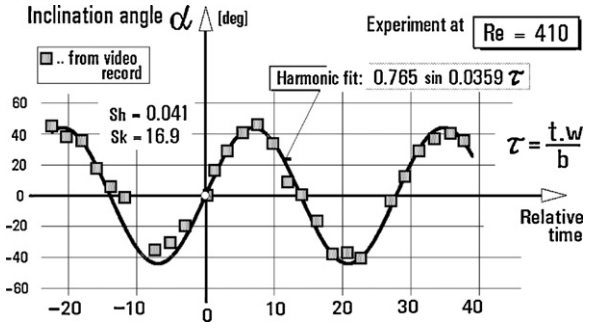

Fig. 15. Periodic variation of the inclination angle α of the demarcation line slope (defined in Fig. 14) as it was measured in the frames of the video clip. It was by fitting the harmonic dependence that the oscillation frequency for experiment G with model M1 was determined.

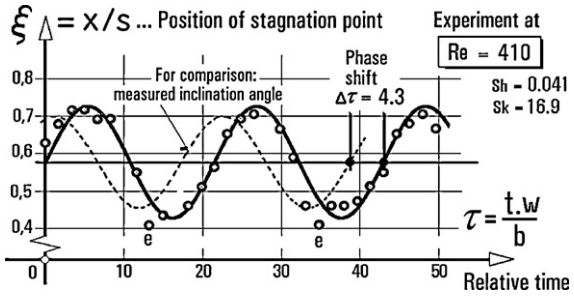

Fig. 16. Also varying periodically is the relative magnitude of the distance x (Fig. 14). Systematic deviations of the point "e" suggests the oscillation may be not simply harmonic.

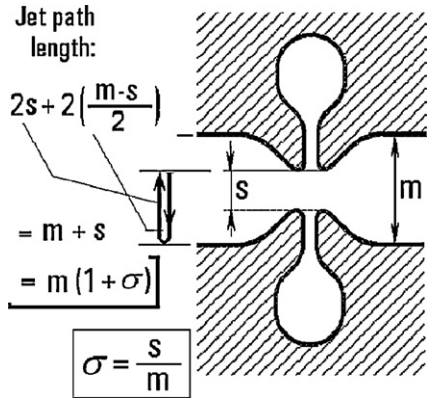

Fig. 17. Extremely simplified expression for the feedback loop length used – together with measured jet velocity – in the kinematic model of the oscillation.

This ignores the jet motion in the transversal direction, so that the values resulting from the approximation are certainly shorter than the real flowpath. The corresponding shorter travel time may be partly compensated by the neglect of the decrease of the real jet velocity along the loop. This approximation also assumes the jet moves up to the opposite wall of the exit channel before it is turned back, which it does not – as seen e.g. in Fig. 9. Nevertheless, the simplification leads to quite simple expression for the period

$$\Delta t_p = \frac{2b}{\beta w}(1+\sigma) = \frac{2\,\text{jet path lengths}}{\text{nozzle exit velocity}} \tag{8}$$

for oscillation frequency

$$f = \frac{1}{\Delta t_p} = \frac{\beta w}{2b(1+\sigma)} \tag{9}$$

and Strouhal number

$$Sh = \frac{f\,b}{w} = \frac{\beta}{2(1+\sigma)} \tag{10}$$

The non-dimensionalised frequency in Eq. (10) is dependent solely upon the geometric parameters β and σ, defined in Fig. 5. In the experiment G with the model M1, characterised by the nozzle width $b = 3.4$ mm, these parameters were

$$\beta = 0.15 \tag{11}$$

$$\sigma = 0.46 \tag{12}$$

and the idealised jet path

$$\frac{b}{\beta}(1+\sigma) = 33.1\,\text{mm} \tag{13}$$

The nozzle-exit velocity, evaluated from the flow rate measured by flowmeter, was

$$w = 0.118\,\text{m/s} \tag{14}$$

so that from Eq. (9) the theory predicts frequency

$$f_{\text{theor}} = 1.783\,\text{Hz} \tag{15}$$

Actually measured frequency, evaluated by the harmonic fit in Figs. 15 and 16, was

$$f = 1.618\,\text{Hz} \tag{16}$$

It is possible to improve upon the accuracy of these expressions by introducing an additive correcting term μ of the order 1.0, evaluated from comparisons with experimental data. Apart from taking into account the longer, curved path that the jet travels, it also represents an allowance for the variations (decrease) of the jet velocity along its path, as well as for the fact that oscillation period, due to the finite jet switching time, is not simply equal to two travel times. The corrected jet path, replacing Eq. (13), is then

$$m(\mu+\sigma) = \frac{b}{\beta}(\mu+\sigma) \tag{17}$$

whereby the expressions in Eqs. (8)–(10) are replaced by

$$\Delta t_p = \frac{2\,b}{\beta w}(\mu+\sigma) \tag{18}$$

$$f = \frac{1}{\Delta t_p} = \frac{\beta w}{2b(\mu+\sigma)} \tag{19}$$

$$Sh = \frac{f\,b}{w} = \frac{\beta}{2(\mu+\sigma)} \tag{20}$$

In the case of the experiment G discussed above, the prediction may be brought into perfect correspondence with the experimental observation using the corrected version of the expressions with

$$\mu = 1.1489 \tag{18'}$$

the required correction of slightly less than mere 15% is a remarkable success for the so simple theory.

Plausibility of this theory was further increased when it was found that it is possible to predict with a reasonably small error also the oscillation frequency found in experiments with the model M2, in its various versions with different aspect ratios.

Of course, the neglect in the theory of the friction effect influencing the jet motion at small aspect ratios is one of the obvious weaknesses of this approximation.

The experimental evaluations of the oscillation frequency – again by analysis of video clips – in the M2 case, at velocity ratio wA/wB = 1, found the oscillation period to depend on the aspect ratio λ quite significantly. The experimental runs were made with $\lambda = 1.25$ and $\lambda = 2.5$ at several different flow velocities in each case. The results are presented in Fig. 18. As expected, with both λ values the frequency increased with increasing velocity, in agreement with the idea of typical trend of constant Strouhal number *Sh*. Also predictable was the fact that reliable, regular oscillation required higher flow rates – and in Fig. 18 higher Reynolds numbers – in the version with the smaller aspect ratio λ.

The increase of frequency with flow rate, however, was discontinued by an unexpected change apparent in Fig. 18: the oscillation frequency levelled off and remained constant at f_{res} – or at its higher multiple. This was explained by the rather sensitive processes in the oscillator becoming locked to an external resonant effect. Later, this resonance was discovered to be a parasitic effect, caused by

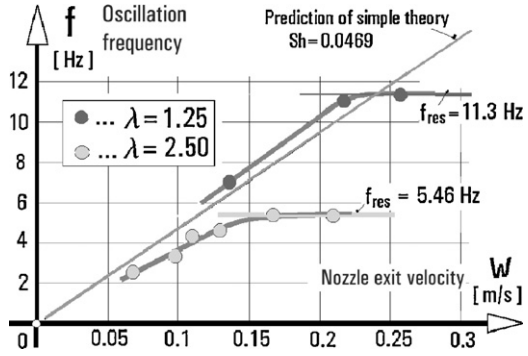

Fig. 18. Dependence of oscillation frequency on the nozzle exit velocity found by analysis of video clips of experiments with the model M2. The kinematic theory discussed above predicts a monotonous linear growth, equal for any aspect ratio λ. Actual data show an influence of λ and a locking-in to a parasitic resonance in the outlets.

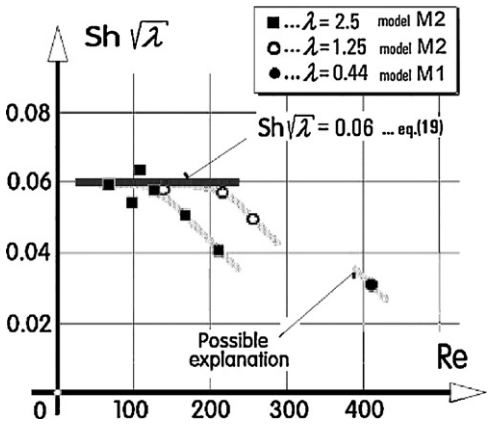

Fig. 19. The universal expression for the oscillation frequency – expressed in the dimensionless form of Strouhal number *Sh* – valid for any aspect ratio λ as long as the conditions avoid the locking to a parasitic resonance. The behaviour of the model M1 could be brought into general agreement by the explanation that it was also influenced by the locking – of course, with just single available data point the suggested slope is purely hypothetical.

conditions in the U-tube inadvertently set up in the connection tubes Thus only the results at lower Reynolds numbers should be considered.

In the results with the model M2, the influence of λ could be eliminated if the results were plotted with the frequency multiplied by the square root the aspect ratio – Fig. 19. Thus the generally applicable scaling law for mixers geometrically similar in plan but having different depths h of the cavities may be written as.

$$Sh\sqrt{\lambda} = 0.06 \tag{19'}$$

4.2. Generated layered structures

All micromixers generate interleaved thin layers – or slender columns – of the two mixed fluids and so does also the discussed oscillator when used as a mixer. Even though the actual shape of the layers is far from simple (cf. Fig. 10) the conceptual model of Fig. 3 may be useful. It is desirable to have the layer thickness δ as small as possible, to make easier the final Fickian blending within an available length l of the connected channel (Fig. 2). The process of generating and depositing the layers in the exit channel may be modelled quite simply: the time it takes for a layer to form is one half of the oscillation period Δt_p. During this time, the flow in the exit channels travels the distance $w_p\ \Delta t_p/2$, dependent upon the flow velocity w_p in the exit channel. Even though complicated velocity profile is likely to by develop (Fig. 20), in the simplified approximation it is possible to assume constant velocity across the cross section equal to the nozzle exit velocity w multiplied by the area ratio β.

$$w_p = \beta w \tag{20'}$$

Non-dimensionalised with respect to the nozzle width b, the resultant expression for the relative layer thickness is simply:

$$\frac{\delta}{b} = \mu + \sigma \tag{21}$$

obtained by inserting the expression for Δt_p from Eq. (17). This linear law of layer formation is supported by experimental results shown in Fig. 21.

With the numerical values for experiment G, the theoretical prediction is:

$$\frac{\delta}{b} = 1.6 \tag{22}$$

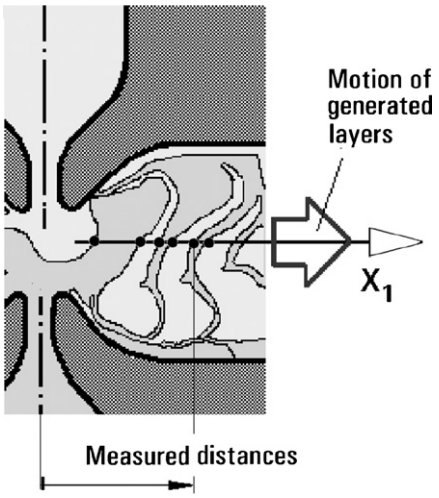

Fig. 20. Positions of the boundary between the two fluids were determined in the frames of the video record of the experiment G with model M1. They were made clearly distinguishable by the posterisation. With known frame-capturing frequency of the camera, the data provided interesting information about the generated lamellae.

while the linear fit through the experimental values in Fig. 21 resulted in

$$\frac{\delta}{b} = 1.53 \tag{23}$$

this represents a remarkably small, only 4% error.

What is really needed in the applications may be best expressed by means of the volume V of the lamella formed in one output channel. It is evaluated as the volume flow rate passing through one of the nozzles delivered into the channel during one oscillation period. Since the fluid flows there, with velocity w through the rectangular area bh during only one half of the period, the volume is

$$V = \frac{1}{2f} w\, bh \tag{24}$$

For the experiments performed with the model M2, its magnitudes are plotted in Fig. 22.

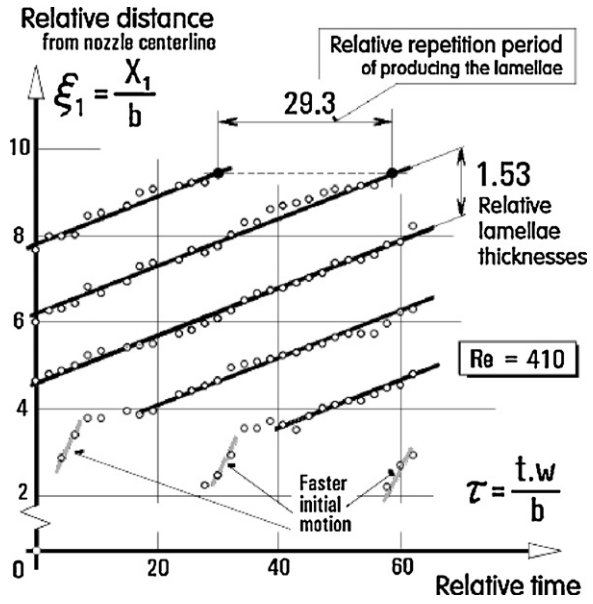

Fig. 21. Measured positions of the interfaces, Fig. 20, in individual frames of the video record of the experiment G with model M1, provide information about the thickness δ of the generated layers as well as their propagation in the exit channel.

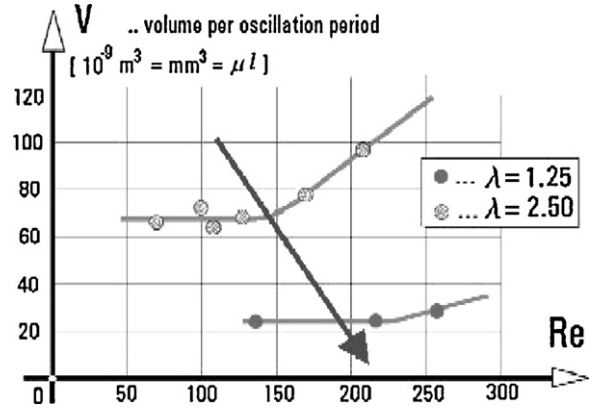

Fig. 22. Volume of one of the two fluids delivered during one oscillation period into the exit channel of the model M2. For easier elimination of concentration gradient before the entry into the microreactor, the volume has to be as small as possible. This is, perhaps somewhat surprisingly, better achieved with the smaller aspect ratio λ.

Using the definition of aspect ratio λ, the volume is

$$V = \frac{1}{2f} w \lambda b^2 \tag{25}$$

$$\frac{f\,b}{w}\sqrt{\lambda} = 0.06$$

By invocation of Eq. (19), deposited as a layer across the exit channel in one period is therefore

$$V = \frac{1}{0.12}\left(b\sqrt{\lambda}\right)^3 \tag{26}$$

Somewhat surprisingly, the ways towards making the volume V small are:

- decreasing mixer size (characterised by the nozzle exit width b), or
- decreasing the aspect ratio λ

5. Conclusions

Micromixers in general generate in their exit channels thin layers (or, in general, small volumes V) of the two fluids placed side by side. The design discussed here achieves this by an operation periodic in time – performed in a very simply shaped cavity, easy to make by micromanufacturing. Apart from the mixing, the design may be used with mutually immiscible liquids for producing monodisperse emulsions or for liquid–liquid extraction. Despite the extreme simplicity of the device geometry, the mechanism of the oscillation is obviously rather complex – and in the experiments that could be made it was unfortunately obscured by a parasitic resonance. Nevertheless, based on a drastically simplified hypothesis of the jet forming a vortical feedback loop, an extremely simple (actually only kinematic rather than dynamic) theory explaining the device behaviour was set up and its predictions were found to be in agreement with the experimental findings, within reasonably small errors.

Experiments performed with two – mutually very similar but of different size – scaled-up models demonstrated capability of operating at Reynolds number of the order as low as 10–100, which is less than the typical demands placed on mixers, which usually supply a number of microreactors.

Unfortunately, the support for this research was terminated – and the author also had to return to his home country – before a complete systematic parameter study could be performed. The usefulness of the device seems, however, to be without doubt and its advantages are such that they deserve reporting the findings from even such a not finalised project.

Acknowledgments

Support by research grant Nr. IAA200760705 from the Grant Agency of the Academy of Sciences of the Czech Republic, by the grant N. 101/07/1499 from the Grant Agency of the Czech Republic, and by the research plan AV0Z20760514 are gratefully acknowledged. The underlying phenomenon was discovered – and initial investigations of it were performed – while the author stayed in the Department of Chemical and Process Engineering at the University of Sheffield, U.K. Collaboration with Dr. J.R. Tippetts and students Y.Y. Low and M. Winter there was particularly crucial for the experimental investigations.

References

[1] V. Tesař, Pressure-driven microfluidics, ISBN-10: 1596931345, Artech House Publishers, Boston, MA, USA, 2007.
[2] W. Ehrfeld (Ed.), Microreaction technology: industrial prospects, ISBN 3-540-66964-7, Springer, Berlin, 2000.
[3] J.-C. Charpentier, Process intensification by miniaturization, Chemical Engineering and Technology 28 (3) (2005) 255–258, March.
[4] S. Hardt, K.S. Drese, V. Hessel, F. Schönfeld, Passive micromixers for applications in the microreactor and μTAS fields, Microfluidics and Nanofluidics 1 (2005) 108.
[5] C.J. Campbell, B.A. Grzybowski, Microfluidic Mixers: from Microfabricated to Self-Assembling Devices, Phil. Trans. Royal Society, London, 2004.
[6] V. Mengeaud, J. Josserand, H.H. Girault, Mixing processes in a zigzag microchannel: finite element simulations and optical study, Analytical Chemistry 74 (2002) 4279.
[7] S. Hardt, H. Pennemann, F. Schönfeld, Theoretical and experimental characterization of a low-Reynolds number split-and-recombine mixer, Microfluidics and Nanofluidics 1 (2005) 237.
[8] V. Tesař, Y.Y. Low, Study of shallow-chamber vortex mixers for microchemical applications, in: Proceedings of 9th International Symposium on Flow Visualization, Edinburgh, paper No. 445, August, 2000.
[9] V. Tesař, Y.Y. Low Microfluidic mixing based upon interfacial instability, Proceedings of Colloquium Fluid Dynamics 2000, ISBN 80-85918-45-5, pp. 59, published by Inst. of Thermomechanics, Academy of Sciences of the Czech Republic, Prague, October 2000.
[10] V. Tesař Asymmetric bistability and oscillation phenomena in colliding jet flows – in Czech, Proceedings of Colloquium FLUID DYNAMICS'99, Prague, Czech Rep., published by Inst. of Thermomechanics AS CR, ISBN 80-85918-52-8, pp.213–218, October 1999.
[11] V. Tesař Microfluidic turn-down valve, Journal of Visualisation, Vol.5, No.3, p. 301, ISSN 1343-8875 2002.
[12] V. Tesar, J.R. Tippetts, R.W.K. Allen Microfluidic Mixer, in Particular for Reactant Mixture Preparation for Chemical Microreactors, British Patent Application WO 01/28670Al, June 2000.
[13] V. Tesař, J.R. Tippetts, Y.Y. Low, Oscillator mixer for chemical microreactors, in: G.M. Carlomagno, I. Grant (Eds.), Proceedings of 9th International Symposium on Flow Visualization, Edinburgh, paper No. 298, August, 2000.
[14] O.M. Wilkin, R.W.K. Allen, P.M. Mailtlis, J.R. Tippetts, V. Tesař, M.L. Turner, A. Haynes, M.J. Pitt, Y.Y. Low, B. Sowerby, High throughput testing of catalysts for the hydrogenation of carbon monoxide to ethanol, in: E.G. Derouanne, et al. (Eds.), Principles and Methods for Accelerated Catalyst Design and Testing, 299-303, ISBN 1402007205, Kluwer Acad. Publishers, the Netherlands, 2002.
[15] V. Tesař, K. Peszyński, Microfluidic oscillator for generating oil/water emulsions, Pneumatyka, May–June, 3(34) ISSN 1426-6644 p. 8, Poland, 2002.
[16] V.A. Denshchikov, V.N. Kondratev, A.N. Romashov, V.M. Chubarov, Auto-oscillations of planar colliding jets, Fluid Dynamics 18 (3) (1983) 460.
[17] A. Nomoto, K. Yamamoto, Y. Ohshio, Axial impingement of two bounded jets, in: Proceedings of 2nd International JSME Symposium on Fluid Machinery and Fluidics (Tokyo), 1972, p. 71.
[18] D.A. Johnson, P.E. Wood, Self-sustained oscillations in opposed impinging jets in an enclosure, Canadian Journal of Chemical Engineering 78 (2000) 867, ISSN 0008-4034.
[19] J. Gregory, J. Sullivan, S. Raghu, Jet interaction studies in a fluidic oscillator, in: Proceedings of 58th Annual Meeting of the Division of Fluid Dynamics, Chicago, IL, November, 2005.
[20] R.S. Brodkey, A. Yusuf, A. Brown, M. Garcia, Y. Zhao, J. Knight, T. Yang, M. Nilsen, Novel computational and experimental methods in mixing, in: AIChE Annual Meeting, Conference Proceedings, 2005, p. 3973.

[21] V. Tesař, C.-H. Hung, W. Zimmerman, No-moving-part hybrid-synthetic jet actuator, Sensors and Actuators A 125 (2) (2006) 159, 10 January.
[22] V. Tesař, Z. Trávníček, J. Kordík, Z. Randa, Experimental investigation of a fluidic actuator generating hybrid-synthetic jets, Sensors and Actuators A 138 (2007) 349.
[23] V. Tesař, Microfluidic systems for combinatorial chemistry, in: L. Dongqing (Ed.), Encyclopedia of Microfluidics and Nanofluidics, Springer, 2008, pp. 1221–1230, ISBN: 978-0-387-48998-8.
[24] C.D. Armeniades, W.C. Johnson, T. Raphael, Mixing Device, United States Patent No. 3 286 992, filed November. 29, 1965.
[25] V. Tesař, Fluid plug microfluidic valve for low Reynolds number fluid flow selector units, Journal of Visualization 6 (1) (2003) 77.
[26] R.F. Boucher, Low Reynolds number fluidic flowmetering, Journal of Physics E–Scientific Instruments 21 (1988) 977.
[27] V. Tesař, J. Barker, Dominant vortices in impinging jet flows, Journal of Visualisation Japan 5 (2) (2002) 121.
[28] S. Kida, M. Tanaka, Dynamics of vortical structures in a homogeneous shear flows, Journal of Fluid Mechanics 274 (1994) 43.
[29] H. Schade, A. Michalke, Zur Enststehung von Wirbeln in einer freien Grenzschicht (On formation of vortices in a free shear layer – in German), Zeitschrift für Flugwissenschaften 10 (1962) 147.